Interface Focus

Interface Focus (2011) **1**, 490–502
doi:10.1098/rsfs.2011.0017
Published online 6 May 2011

Review

Ultrasonic colour Doppler imaging

David H. Evans[1,*], Jørgen Arendt Jensen[2] and Michael Bachmann Nielsen[3]

[1]*Department of Cardiovascular Sciences, University of Leicester, Leicester, UK*
[2]*Center for Fast Ultrasound Imaging, Department of Electrical Engineering, Technical University of Denmark, 2800 Lyngby, Denmark*
[3]*Department of Radiology, Section of Ultrasound, Rigshospitalet, Blegdamsvej 9, 2100 Copenhagen Ø, Denmark*

Ultrasonic colour Doppler is an imaging technique that combines anatomical information derived using ultrasonic pulse-echo techniques with velocity information derived using ultrasonic Doppler techniques to generate colour-coded maps of tissue velocity superimposed on grey-scale images of tissue anatomy. The most common use of the technique is to image the movement of blood through the heart, arteries and veins, but it may also be used to image the motion of solid tissues such as the heart walls. Colour Doppler imaging is now provided on almost all commercial ultrasound machines, and has been found to be of great value in assessing blood flow in many clinical conditions. Although the method for obtaining the velocity information is in many ways similar to the method for obtaining the anatomical information, it is technically more demanding for a number of reasons. It also has a number of weaknesses, perhaps the greatest being that in conventional systems, the velocities measured and thus displayed are the components of the flow velocity directly towards or away from the transducer, while ideally the method would give information about the magnitude and direction of the three-dimensional flow vectors. This review briefly introduces the principles behind colour Doppler imaging and describes some clinical applications. It then describes the basic components of conventional colour Doppler systems and the methods used to derive velocity information from the ultrasound signal. Next, a number of new techniques that seek to overcome the vector problem mentioned above are described. Finally, some examples of vector velocity images are presented.

Keywords: ultrasonic colour Doppler; imaging; clinical applications

1. INTRODUCTION

Standard ultrasonic pulse-echo (PE) imaging generates anatomical cross-sectional images of the body (figure 1). In the case of ultrasound colour flow imaging (CFI) (known also as colour Doppler imaging), a colour map depicting movement is superimposed on the PE image (figure 2). The technique has many applications but is mainly used to image blood flow, and to a lesser extent movement of the cardiac muscle. A brief introduction to some clinical applications of CFI is given in §2. In principle, CFI techniques are similar to PE techniques in which information regarding the location of each target in the body, corresponding to each pixel in the image, is derived in the same way, i.e. from a knowledge of ultrasonic beam direction and pulse round-trip transit time, but the returning echoes are analysed in terms of Doppler shift rather than amplitude. Although the technique is often described as a Doppler technique, it does not make use of the Doppler shift on each transmitted pulse, but rather generates estimates of velocity from the phase shifts or time delays between echoes from the same sample volume during subsequent pulses. A rate of change of phase can be interpreted as a frequency shift and the velocity of the target can be calculated from this frequency shift using the same equation that is used to interpret the true Doppler shift found in continuous wave ultrasound instruments, i.e.

$$f_{\mathrm{d}} = \frac{2f_{\mathrm{t}}|v|\cos\Theta}{c}, \tag{1.1}$$

where f_{d} is the Doppler shift frequency, θ is the angle between the ultrasound beam and flow vector, $|v|\cos\Theta$ is the component of the velocity of the target towards the transducer, f_{t} is the transmitted ultrasound frequency and c is the velocity of ultrasound in the tissue. Note therefore that in standard CFI applications, it is the component of the velocity of the

Author for correspondence (dhe@le.ac.uk).

One contribution of 15 to a Theme Issue 'Recent advances in biomedical ultrasonic imaging techniques'.

Received 23 February 2011
Accepted 12 April 2011

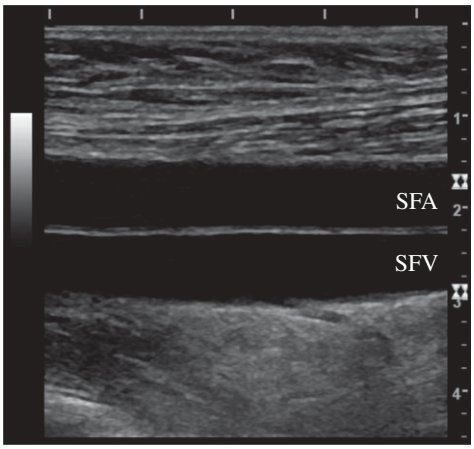

Figure 1. Pulse-echo image of the superficial femoral artery (SFA) and the superficial femoral vein (SFV) in the thigh of a healthy subject. The scan direction is vertical to generate the best view of the arterial walls. The scale to the right and the top of the image is calibrated in centimetres.

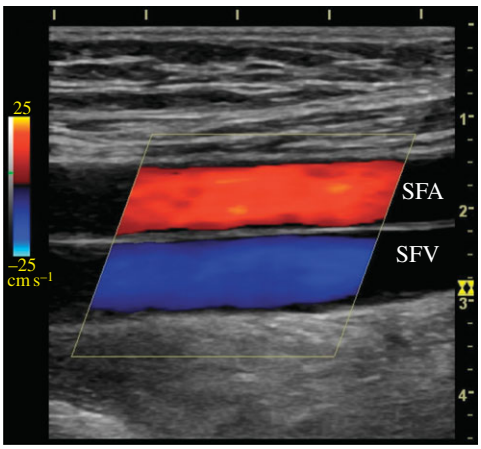

Figure 2. Colour flow image obtained by superimposing Doppler information on the pulse-echo image. The subject's head is to the left of the scan, and so the arterial flow is from left to right and the venous flow from right to left. The colour scale on the left of the image is calibrated in cm s^{-1}, and shows that flow towards the probe is coloured as red-orange-yellow, while flow away from the probe is coloured in shades of blue. Note that the area of the colour box indicating the region from which velocity information is extracted occupies only part of the image. Note also that the angle of the colour box is inclined at an angle to the vertical to ensure that the Doppler angle is different from 90°.

target towards the transducer that is measured and therefore additional information about the direction of flow is necessary if the velocity vector is to be quantified in terms of magnitude and direction.

Although the CFI technique has many similarities to the PE technique, it is much more technically demanding for a number of reasons. Firstly, the most common target for CFI is blood rather than solid tissue as in PE, and the magnitudes of echoes from blood may be several orders of magnitude less than those from solid tissue. Secondly, in PE, it is only necessary to interrogate a target with a single pulse of ultrasound to determine its position, but in CFI the target has to be interrogated several times in order to determine its velocity. While, in principle, it should be possible to calculate velocity from just two pulse transmissions, in practice, many more are required to generate a good estimate, partly because of the stochastic nature of echoes from blood but also because it is necessary to filter the returning signal from blood to reject the very much larger signals from the surrounding solid tissues (which also move, but in general with a much lower velocity). Because of the finite velocity of ultrasound, the requirement to sample a target a number of times imposes limitations on the number of scan lines that can be used to form each image, or the frame rate (or both), and quite frequently the colour box (figure 2) does not extend over the entire PE image.

In what follows, we describe some examples of clinical applications of CFI, provide an overview of conventional CFI systems and finally examine some of the limitations of the current CFI systems and emerging techniques that may overcome these limitations.

2. SOME CLINICAL APPLICATIONS OF COLOUR FLOW IMAGING

The introduction of CFI was a major breakthrough in medical ultrasound imaging. Previously, pulsed-wave spectral Doppler had allowed the sampling of velocities from a single sample volume within the body (the operator being able to select the sample volume with reference to a cursor placed on the PE image), but CFI allows velocities to be imaged simultaneously over a region of interest, allowing the rapid identification of the presence and direction of flow, highlighting gross circulation anomalies, and depicting the location of stenoses and occlusions. Ultrasound CFI can be used in any vessel depicted in the PE image, subject to it being possible to achieve a suitable Doppler angle, although deep vessels can be more difficult to image both because of sensitivity issues (owing to attenuation by overlying tissues) and because of the increased inter-pulse interval necessary for the ultrasound pulses to make a round-trip from the transducer to the target (extended inter-pulse intervals, i.e. a decreased pulse-repetition frequency, may lead to inadequate sampling of the Doppler signal resulting in aliasing or misinterpretation of the Doppler shift frequency). Ultrasound CFI has been found to be useful in many areas of vascular investigation, a small sample of which are mentioned below. It is worth noting that in many applications, CFI is used to generate an overall representation of blood flow and to identify specific areas from which spectral Doppler measurements, which give more quantitative data, can be made.

2.1. Carotid artery stenosis

A common cause of stroke is the shedding of emboli (small solid particles such as platelet aggregates or atheromatous plaque) from stenoses (narrowings) in the carotid arteries of the neck. These emboli become wedged in end-arteries in the brain and cause regions of the brain to infarct. Although at one time, the gold standard investigation for detecting such stenoses was invasive X-ray angiography, the diagnostic test itself was shown to cause embolization and stroke, and now

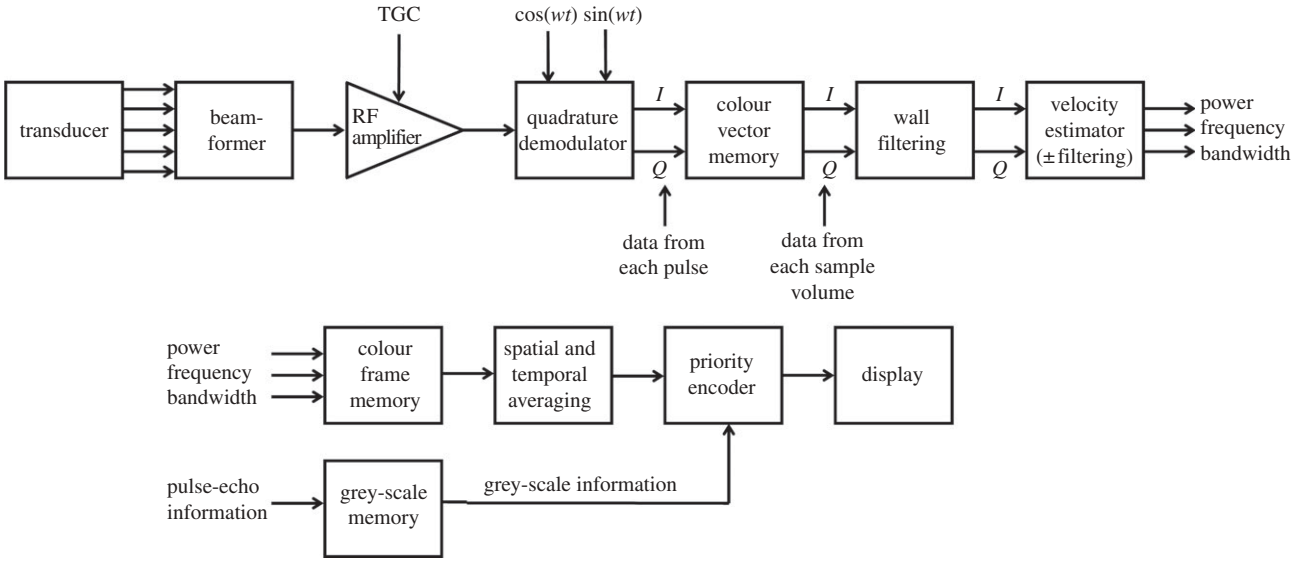

Figure 3. General layout of the receive Doppler path for a colour flow imaging system (RF, radio frequency; TGC, time gain compensation; *I*, in-phase components of each signal; *Q*, quadrature components of each signal).

the method of choice for the assessment of such vessels is CFI together with duplex sonography (i.e. PE imaging together with spectral Doppler), and most carotid artery surgery now takes place based on the ultrasound examination alone. The grading of the stenosis is based on the maximum velocities recorded in the arteries rather than the geometry recorded by PE imaging [1]. Although the technique works extremely well, velocity estimates are based on the assumption that blood flow is parallel to the artery wall, whereas in practice, flow patterns in the carotid artery can be very complex (see [2]), and it is possible that these measurements can be refined further in the future using vector velocity techniques such as those described in §4.3.

2.2. Renal artery stenosis

One cause of increased systemic blood pressure is renal artery stenosis. The diagnostic gold standard for the detection of renal artery stenosis is angiography, but this cannot be used for the routine screening of hypertensive patients as it is invasive, and because of the hazards associated with ionizing radiation exposure and X-ray contrast agents. Ultrasound CFI, on the other hand, is totally non-invasive and is good at detecting haemodynamically significant stenoses [3,4]. In the case of patients with renal insufficiency, CT and MR angiography are contraindicated because of the risk of contrast-induced nephropathy and nephrogenic systemic fibrosis, respectively. While CFI and duplex sonography have become established as the methods of choice for the diagnosis of renal artery stenosis, the method can be time-consuming, because the insonation angle of the proximal part of the renal arteries is close to 90°, and it is anticipated that in the future, vector velocity imaging may help to speed up examination times.

2.3. Others

Some other important applications of CFI are the assessment of acute and chronic deep venous thrombosis and venous insufficiency [5], the diagnosis of portal vein thrombosis [6], the assessment of portal hypertension [7] and in the assessment and follow-up of transplanted organs where various complications can be identified.

3. CONVENTIONAL COLOUR DOPPLER IMAGING SYSTEMS

The detailed layout of CFI systems varies from one machine to another, but all contain similar building blocks. Figure 3 illustrates one possible configuration. Nearly all modern CFI systems use array transducer technology, where the transducer consists of a large number of individual elements capable of transmitting and receiving ultrasound pulses. The purpose of the beam-former during transmission is to apply the correct combination and sequence of signals to the individual transducer elements to generate a suitable transmitted beam, and, during reception, to combine the returning echoes in the correct way to generate the appropriate receive beam. The output from the beam-former is amplified in a time-dependent manner (to compensate for the additional attenuation experienced by echoes from deep within the body), and then quadrature-demodulated to generate the in-phase (*I*) and quadrature (*Q*) components of the Doppler signal. In the schematic shown, the demodulated signals are stored in a colour vector memory before being filtered and processed to extract the power, mean frequency and bandwidth of the Doppler signal returning from each tissue sample volume. These signals are further processed and then combined with PE imaging data to generate a combined display of both anatomical and velocity information (figure 2).

3.1. Beamforming

As for PE imaging, dedicated electronics control the aperture size, the apodization, the steering and the focus of both the transmitted and received ultrasound beams. However, the pulsing sequence, the scan area

and the angle of insonation may all differ. As already mentioned, while it is only necessary to transmit and receive one pulse to determine the position of a target, many more are required to estimate the component of velocity towards the transducer (typically between 8 and 16) and thus there is a trade-off between the colour frame rate and the region of tissue interrogated for motion, both laterally and axially. The ideal sampling rate for CFI depends on the Doppler frequency being detected. In order to avoid aliasing, the sampling frequency must exceed the Doppler frequency itself (assuming that both quadrature signals are sampled otherwise twice the Doppler frequency) but must not be so high that little phase-change takes place between adjacent samples, in which case the velocity estimate will be associated with a large variance. Because of the latter consideration, individual colour lines may not be assembled from adjacent pulses but from interleaved pulses. The beam angles used for CFI may also differ from that used for PE imaging (during the same scan) in order to minimize the Doppler angle, which has the dual advantage of maximizing the Doppler shift frequency and reducing the error in velocity calculations made using $\boldsymbol{\Theta}$. This technique is frequently used when imaging superficial vessels that lie parallel to the skin surface, as the best images of the vessel walls are obtained by transmitting and receiving pulses at right angles to the walls, but in order to image the flow in the vessel, the pulses must be transmitted and received at an angle that is non-perpendicular to the vessel axis. Beamforming technology has been reviewed by Angelsen *et al.* [8], Thomenius [9] and Whittingham [10].

3.2. Filters

One of the most challenging aspects of CFI is the rejection of echoes from stationary or nearly stationary tissue, which can be much larger than those from the intended target. This is particularly so where the target is blood, in which case the unwanted clutter signal from solid tissues can exceed the signal from blood by 40–60 dB [11–13]. The problem is similar to that found in both continuous-wave and pulsed-wave Doppler, but is significantly more difficult to resolve in CFI applications because of the low number of samples available for analysis.

The simplest type of clutter rejection filter is the single echo canceller, where each new echo is subtracted from its predecessor—thus, any echo from a stationary target is cancelled, while echoes from moving targets are preserved. Unfortunately, this simple technique is not adequate in CFI applications because of its poor roll-off characteristics (6 dB per octave) and wide transition band. The roll-off characteristics can be improved by cascading two such filters, but this only increases the transmission band problem. Other more complex finite impulse (FIR) filters can be designed, but in order to achieve the performance necessary for CFI, a large number of data samples would be required.

The frequency characteristics of infinite impulse response (IIR) filters are considerably better than those of FIR filters, but as their name implies, they have long transient responses, which means that unless appropriate steps are taken to initialize them suitably, a large number of output values need to be discarded before the data becomes valid, something that is not possible in CFI applications because of the short data segments available. Because of this difficulty, various strategies for IIR filter initialization have been proposed (see [14–16]), although unfortunately such schemes may also introduce bias into the subsequent frequency estimation [17,18].

Because of the limitations of the classical FIR and IIR filters in CFI applications, a number of alternative approaches have been explored. These include regression filters, based on the assumption that the slowly varying clutter components of the Doppler signal can be approximated by a low-order polynomial [19–21], and methods based on eigendecomposition [22–28].

A useful review of clutter filter design for CFI has been published by Bjærum *et al.* [21].

3.3. Velocity estimation

Once the clutter signals have been rejected, the I and Q components of the Doppler signal are further processed to generate estimates of power, frequency and bandwidth. As already noted, CFI systems (and indeed pulsed-wave Doppler systems in general) do not use the Doppler shift frequency of individual pulses of ultrasound; this is because other mechanisms such as frequency-dependent attenuation and frequency-dependent scattering significantly change the spectrum of the pulse and make it impossible to estimate the change due simply to the Doppler effect. Instead, CFI systems rely on estimating the rate of change of phase of the signal returning from a given sample volume, or, alternatively, the change in the round-trip time from the transducer to a defined group of scatterers (identified by their scattering signature). Both methods have been implemented on commercial machines in the past, but nearly all now rely on techniques for estimating rates of change of phase.

A simple model for the change in phase can be derived from using the time shift of the scatterers between pulse emissions [29]. The axial motion Δz along the ultrasound beam between two pulse emissions is equal to

$$\Delta z = |\boldsymbol{v}|\cos(\boldsymbol{\Theta})\, T_{\mathrm{prf}} = v_z\, T_{\mathrm{prf}}, \tag{3.1}$$

where T_{prf} is the time between two pulse emissions. This translates into a time shift t_{s} between the two received signals as

$$t_{\mathrm{s}} = \frac{2v_z}{c}\, T_{\mathrm{prf}}, \tag{3.2}$$

and this delay will increase as a function of emission number i. Emitting a sinusoidal signal will then result in a received signal $r(t,i)$ from a single moving scatterer given by

$$\begin{aligned} r(t,i) &= a\sin\left(2\pi f_{\mathrm{t}}\left(t - \frac{2D}{c} - it_{\mathrm{s}}\right)\right) \\ &= a\sin\left(2\pi f_{\mathrm{t}}\left(t - \frac{2D}{c} - \frac{2v_z}{c}\, iT_{\mathrm{prf}}\right)\right) \end{aligned} \tag{3.3}$$

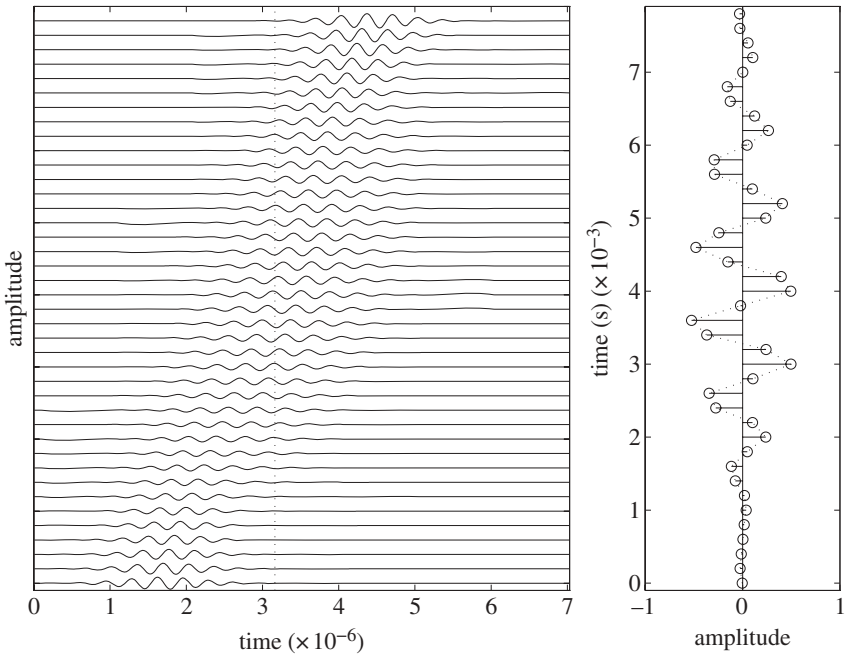

Figure 4. Signal obtained from a single moving scatterer crossing a beam from a concave transducer (from Jensen [29]). Here, the measurement time t_m is indicated on the left panel as the dotted line.

where D is the initial depth of the scatterer and a the amplitude of the scattered signal. Setting the measurement time to a fixed value t_m corresponding to a fixed measurement depth gives

$$r(t_m, i) = a\sin\left(2\pi f_t\left(t_m - \frac{2D}{c} - it_s\right)\right)$$
$$= -a\sin\left(2\pi\frac{2v_z}{c}f_t iT_{prf} - \phi_m\right), \qquad (3.4)$$

where iT_{prf} now corresponds to sampling time and $\phi_m = 2\pi f_t(t_m - (2D/c))$ is a fixed-phase factor. The frequency f_p of the received signal is, thus, directly proportional to axial blood velocity and is given by:

$$f_p = \frac{2v_z}{c}f_t. \qquad (3.5)$$

This is also illustrated in figure 4. The signal from a single scatterer passing the sampling point is illustrated. On the left is seen the individual received radiofrequency (RF) signals, and on the right the sampled signal from extracting one sample from each RF line at the depth of interest. The shape of the pulse is preserved on the right, and its frequency is determined by how fast the scatterer passes the sampling point. A large velocity will compress the pulse and give a high frequency, and a low velocity will elongate the pulse and result in a low frequency.

After complex demodulation and sampling, the received signal r_c can be written as

$$r_c(i) = a\exp\left(-j2\pi\frac{2v_z}{c}f_t iT_{prf} - \phi_m\right)$$
$$= a\exp(-j\phi(i)) = I(i) + jQ(i). \qquad (3.6)$$

As for clutter rejection, the small number of samples available for each frequency estimate presents a number of technical challenges, and although a number of algorithms have been suggested as being useful for estimating the derivative of phase [30], by far the most widely used (with certain modifications) is the autocorrelation technique introduced by Namekawa *et al.* [31] and Kasai *et al.* [32]. The expression for frequency estimation using this technique can be derived using simple geometrical considerations that provide an intuitive understanding of its operation. Figure 5 illustrates the position of a rotating signal vector during two adjacent samples $i-1$ and i, with in-phase components $I(i-1)$ and $I(i)$, and quadrature components $Q(i-1)$ and $Q(i)$. The angular frequency ω of the rotating vector is defined as its rate of change of phase, or

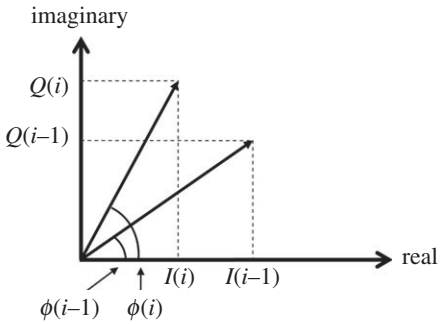

Figure 5. Position of a rotating signal vector during two successive samples $i-1$ and i, showing the in-phase components $I(i-1)$ and $I(i)$ and quadrature components $Q(i-1)$ and $Q(i)$.

$$\omega = \frac{d\phi}{dt} \approx \frac{\phi(i) - \phi(i-1)}{T_{prf}}. \qquad (3.7)$$

The tangent of the phase difference $\phi(i) - \phi(i-1)$ may be written in terms of the ratio of the sine and cosine

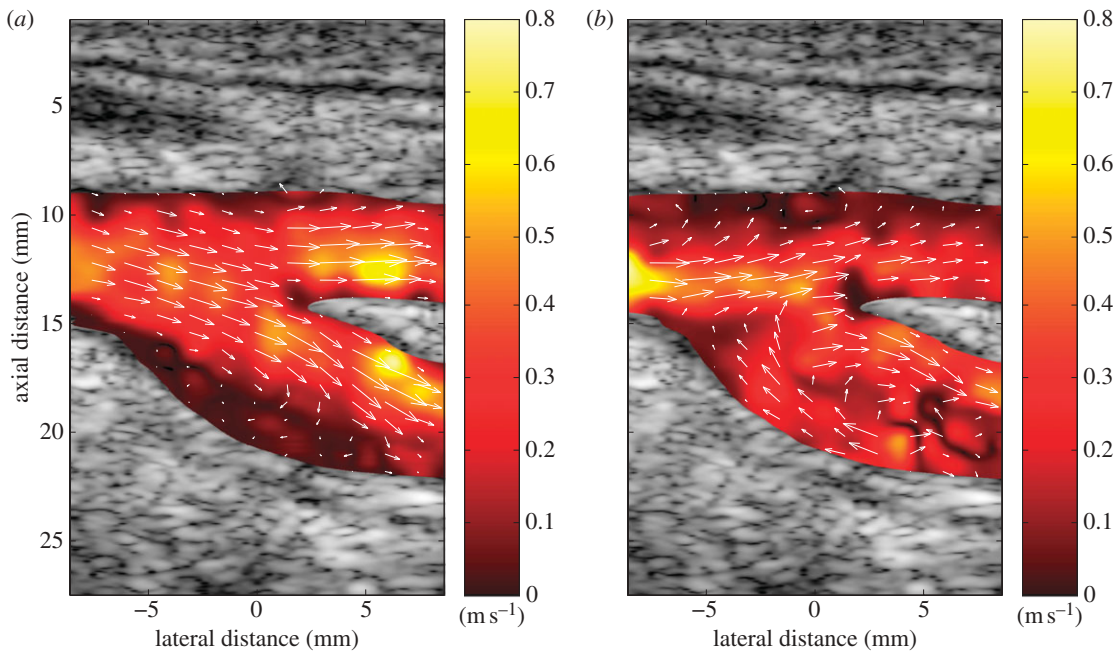

Figure 6. Vector velocity image of the carotid artery bifurcation shortly (*a*) before and (*b*) after peak systole (from Udesen *et al.* [2]). The arrows indicate both direction and magnitude of the velocity and colour intensity indicates velocity magnitude.

of the phase difference according to

$$\begin{aligned}&\tan(\phi(i)-\phi(i-1))\\&=\frac{\sin(\phi(i)-\phi(i-1))}{\cos(\phi(i)-\phi(i-1))}\\&=\frac{\sin\phi(i)\cos\phi(i-1)-\cos\phi(i)\sin\phi(i-1)}{\cos\phi(i)\cos\phi(i-1)-\sin\phi(i)\sin\phi(i-1)}.\end{aligned}\tag{3.8}$$

If the sine and cosine terms are now expressed as the in-phase and quadrature magnitudes of the vectors, and an average frequency calculated by summing over a number of adjacent pulse pairs, then the mean angular frequency can be written as

$$\bar{\omega}=\frac{1}{T_{\mathrm{prf}}}\arctan\left[\frac{\sum_{i=1}^{N}Q(i)I(i-1)-I(i)Q(i-1)}{\sum_{i=1}^{N}I(i)I(i-1)+Q(i)Q(i-1)}\right].\tag{3.9}$$

Formal derivations of the autocorrelation estimator, together with expressions for the variance and average power of the Doppler signal can be found in Jensen [29] and Evans & McDicken [30].

Major advantages of the autocorrelator are that it gives an unambiguous output for narrowband signals over the range of $\pm\pi$ radians, and that it is well behaved with wideband signals with mean frequencies close to $\pm\pi$ radians because it correctly accounts for partial aliasing in a continuous spectrum. The output of the autocorrelation estimator is also ideally unbiased as the addition of white noise to the signal does not affect the autocorrelation at finite lags; unfortunately however, the use of clutter rejection filters will colour the system noise leading to a bias in the mean frequency estimate. This bias can be minimized using clutter filters with good roll-off characteristics.

A significant advance on the simple autocorrelator as a means of quantifying blood flow velocities was introduced by Loupas *et al.* [33,34] and differs from the simple method in two distinct ways. Firstly, the estimate of the Doppler frequency is formed by processing samples from a number of axial depths, and, secondly, the axial velocity is calculated from the Doppler equation using explicit estimates of both the mean Doppler and mean RF frequencies at each range gate location. The two-dimensional autocorrelation estimator has considerable advantages over the conventional one-dimensional method, which implicitly assumes that the mean RF frequency is constant and equal to the centre frequency of the transmitted pulse. In practice, the received RF frequency varies considerably owing to both the stochastic nature of the backscattered signal and the effects of frequency-dependent attenuation and scattering, which lead to perturbations in the Doppler frequency, that tend to track the RF fluctuations [35]. If, on the other hand, velocity is calculated from the ratio of the measured Doppler shift frequency to the measured RF frequency, these effects are at least partially compensated for, and a more stable estimate of velocity obtained. Further details of the two-dimensional autocorrelation estimator, its advantages and its relationship with other estimators can be found in Evans & McDicken [30].

Although methods based on measuring the rates of change of phase and particularly autocorrelation methods are now widely used in commercial machines, colour flow mapping can also be implemented using time domain-based techniques such as cross-correlation [36–39]. These techniques are based on measuring changes in the round-trip time from the transducer to a defined group of scatterers (identified by their scattering signature). To implement this, short segments of the

echo signals from each pulse are compared with similar segments of previous pulses from approximately the same range, to find the best match and hence to estimate the inter-pulse target displacement t_s. It should be noted that this process is not perfect as no two subsequent scattering signatures are identical because of components of motion perpendicular to the ultrasound beam and because of velocity dispersion within the range cell. As for phase-domain techniques, many different time domain-based methods have been explored [39–41] and the reader is referred to Hein & O'Brien [42] and Evans & McDicken [30] for more details.

An interesting variation on correlation-based techniques is the use of decorrelation-based techniques [43], which have been found of value in intravascular applications, where the ultrasound beam is perpendicular to the flow direction and where the scatter from blood is particularly strong because of the high frequencies used.

3.4. Post-processing, priority encoding and display

Once the mean frequency, power and variance of the Doppler signal have been calculated, their values are stored in a colour frame memory before being further processed and combined with PE information to form the final composite image.

Doppler signals are stochastic in nature, which means the estimates of signal parameters vary in a random fashion, and therefore various post-processing techniques such as linear and/or nonlinear, spatial and temporal averaging of the Doppler parameter data are typically employed to prevent rapid fluctuations and drop-out in the final displayed colour images.

For every pixel in the final image (within the region covered by the colour box), there will be both grey-scale PE information and colour Doppler data available. The function of the priority encoder is to determine whether the Doppler data are valid, i.e. whether there is any real flow or movement present, in which case these data are given priority, otherwise the PE data are presented. The details of the priority encoder will vary from machine to machine, but some or all of the following thresholds are likely to be implemented. In many cases, these thresholds will be user-adjustable.

3.4.1. Doppler signal magnitude threshold. If the estimate of average Doppler signal power is less than a minimum threshold level, then only PE information will be displayed. This is because small signals are likely to generate unreliable velocity estimates.

3.4.2. Pulse-echo signal magnitude threshold. If the amplitude of the PE signal is very large, then it is likely to have come from a region containing solid tissue rather than blood and therefore only PE information will be displayed (this does not of course apply in the case of tissue Doppler imaging).

3.4.3. Velocity threshold. If the estimated velocity is very low, it is likely that the Doppler spectrum is dominated by clutter signals that have not been adequately rejected by the high-pass filters and is thus invalid. In this case, only the PE information will be displayed.

3.4.4. Doppler bandwidth threshold. Doppler signals from a small sample volume are likely to have a much smaller bandwidth (corresponding to a small range of velocities) than noise; therefore if the bandwidth exceeds a certain limit, only the PE information will be displayed.

The final composite image data are combined with graphics data (such as patient information, machine setting parameters, distance calibration scales and a colour bar) and written to a video memory and displayed on a display monitor. The colour bar is to assist the interpretation of the colour data and may represent Doppler shift frequency, the component of the velocity towards or away from the transducer, or the relative power of the Doppler signal.

Further information on post-processing can be found in various patents (e.g. [44–47]).

4. NEW TECHNIQUES

CFI was first introduced in the early 1980s and since that time a number of improvements have been made to the method in order to address some of its earlier limitations such as its angle-dependency. This section will describe some of these new developments.

4.1. The need for vector velocity imaging

Conventional colour flow and spectral systems can only determine the motion and hence velocity along the direction of the ultrasound beam. This is very restrictive and a major limitation of the current systems as most major vessels run parallel to the skin surface (figure 1) and the dominant velocity component is, thus, orthogonal to the ultrasound beam. This is currently solved by either tilting the transducer or tilting the ultrasound beam (figure 2). The first approach can often disturb the velocity by pushing on the vessel wall and increasing the velocity. Both approaches capture only part of the velocity as it is given by

$$\hat{v}_z = |\boldsymbol{v}|\cos\boldsymbol{\Theta} = \frac{f_\mathrm{p}}{f_\mathrm{t}}\frac{c}{2}, \tag{4.1}$$

where $\boldsymbol{\Theta}$ is the angle between the beam and the flow vector, f_p is the estimated frequency and f_t is the transducers centre frequency. At an angle of 60°, a velocity of $1\,\mathrm{m\,s^{-1}}$ is depicted as $0.5\,\mathrm{m\,s^{-1}}$; at 80° it is $0.17\,\mathrm{m\,s^{-1}}$. Colour flow systems are therefore not quantitative systems and cannot be used for diagnosis based on a velocity value. Spectral systems are used for this, where the angle problem is solved by changing the angle of a cursor positioned through the range gate to line up with the estimated flow direction. The system then uses information from the cursor angle setting to correct for the $\cos\boldsymbol{\Theta}$ factor. Here, the problem is that the angle can be difficult to judge, and flow is not necessarily parallel to the vessel surface or stationary over the cardiac cycle.

For more complicated geometries such as bifurcations, valves, tortuous vessels and stenoses, the angle will fluctuate over the cardiac cycle. Figure 6*b*

shows a vector velocity image of the bifurcation of the carotid artery shortly after the peak systole. The swirl in the lower branch appears and disappears within 100 ms, wherein the velocity directions change 360°. The angles change throughout the image and over the cardiac cycle and there is no one constant angle. A correct estimation of the velocity must, therefore, be based on finding both magnitude and direction.

4.2. Historical perspective

The angle factor in velocity estimation was recognized early on as a major problem for a true investigation of the circulatory system, and hence many authors have proposed possible solutions. Fox [48] suggested using two crossing beams for finding the velocity in two directions by either employing two transducers or splitting the aperture of an array. From this, both the axial and the lateral velocity components can be calculated. The problem with this approach is that the beams overlap only at one depth when using two, single-element transducers. For electronic arrays, a central beam can be emitted and the receive apertures can track the beam down through the tissue. The angle between the beams, however, decreases as a function of depth and this increases the standard deviation for the lateral velocity component.

Another approach using speckle tracking was devised by Trahey *et al.* [49]. Here, two images or image regions are acquired and one region is correlated to the second to find the displacement of the speckle pattern between the acquisitions. This gives a displacement in both directions and dividing by the time reveals the velocity vector. The major drawback of this approach is that images have to be acquired, which takes a significant time or parallel beamforming has to be employed. Also, the calculation demand is fairly high. Speckle tracking is also used in echo-particle image velocimetry, where a contrast agent is injected into the blood stream and images of the particles are correlated to find the vector velocity [50,51].

A third approach devised by Newhouse *et al.* [52] uses the change in bandwidth of the ultrasound beam. The transition of the scatterers through the beam will change the bandwidth in proportion to the velocity owing to the transit time effect. This can be determined by finding the bandwidth of the received signal. Only few experiments have been published using this approach, and it seems that the bandwidth is affected by a number of factors making it difficult to find the lateral velocity component reliably [53].

Bonnefous [54] suggested using beamforming transverse to the ultrasound field and then cross-correlating signals from several emissions to determine the lateral motion. This approach works if there is solely transverse motion, but a mixture of axial and lateral motion makes the approach break down as the axial signal change dominates. Jensen & Lacasa [55], Jensen [56] and Jensen & Bjerngaard [57] therefore suggested using beamforming along the ultrasound direction and cross-correlation of subsequent acquisitions. A fairly broad beam is emitted and the receive focusing is then performed along the flow direction. The flow angle can be found using a rather elaborate scheme, where all directions are searched and the one with the highest correlation value is the estimated direction [58,59]. This approach is hampered by a very high calculation demand.

A novel approach to vector velocity estimation has been devised by Ohtsuki & Tanaka [60]. They employ a normal CFI image and from this they derive the vector velocity field by calculating a basic flow component and a vortex flow component. The approach has been validated by Uejima *et al.* [61] and several interesting clinical examples are shown by Tanaka *et al.* [62]. The one drawback of the approach is that it relies on the CFI estimates and that turbulence cannot be estimated, as the CFI estimates have to be continuous in space.

A review of the early history of vector Doppler has been published by Dunmire & Beach [63].

4.3. Modern vector velocity imaging

The basic mechanism for finding the velocity in current systems is by estimating the phase shift between two received signals as is done in the autocorrelation approach by Kasai *et al.* [32]. This necessitates a well-defined frequency and this is not the case when the motion is perpendicular to the ultrasound. A novel idea is then to introduce an oscillation in the transverse direction, which causes the received signal to be influenced by a lateral motion as suggested by Munk [64], Jensen & Munk [65] and Anderson [66].

In the transverse oscillation (TO) approach, a multi-element transducer is operated to create such a double-oscillating field (axial–lateral). It should be noted that the monochromatic ultrasound field at the focus can be predicted from the Fourier transform of the aperture function. A uniform excitation (or apodization) of all the elements will give a sinc function and splitting the aperture into two will, thus, give a sinusoidal field, where the lateral oscillation period λ_x is

$$\lambda_x = \frac{2\lambda_z z_0}{d}, \tag{4.2}$$

where d is the distance between the two peaks in the apodization function, z_0 is the depth and λ_z is the axial wavelength. Often, the two peaks are shaped like a Hanning or Gauss curve to limit the extent of the lateral field. The aperture splitting is done on receive, so that the spacing can be increased as a function of space to maintain λ_x constant.

Two beams are focused in parallel in receive from one emission to generate a spatial quadrature signal, so that the direction of the motion can be found. The two beams are spaced $\lambda_x/4$ to yield a spatial quadrature signal. A temporal Hilbert transform is performed on both signals to generate four received signals from which two estimators can give the axial and lateral velocity independently and hence the two-dimensional velocity vector [67].

The received and sampled spatial quadrature signal can be written as

$$r_{\mathrm{sq}}(i) = \cos(2\pi f_{\mathrm{p}} i T_{\mathrm{prf}}) \exp(j 2\pi f_x i T_{\mathrm{prf}}), \tag{4.3}$$

where v_x is the transverse velocity and $\lambda_x = 1/f_x$ is the lateral modulation period. The temporal Hilbert transform of the received signal is

$$r_{\mathrm{sqh}}(i) = \sin(2\pi f_{\mathrm{p}} i T_{\mathrm{prf}}) \exp(j 2\pi f_x i T_{\mathrm{prf}}). \tag{4.4}$$

Two new signals are then formed from

$$r_1(i) = r_{\mathrm{sq}}(i) + j r_{\mathrm{sqh}}(i) \tag{4.5}$$

and

$$r_2(i) = r_{\mathrm{sq}}(i) - j r_{\mathrm{sqh}}(i). \tag{4.6}$$

The estimators are then [67]

$$v_x = \frac{d_x}{2\pi 2 T_{\mathrm{prf}}} \times \arctan\left(\frac{\Im\{R_1(1)\}\Re\{R_2(1)\} + \Im\{R_2(1)\}\Re\{R_1(1)\}}{\Re\{R_1(1)\}\Re\{R_2(1)\} - \Im\{R_1(1)\}\Im\{R_2(1)\}}\right) \tag{4.7}$$

and

$$v_z = \frac{c}{2\pi 4 T_{\mathrm{prf}} f_{\mathrm{t}}} \times \arctan\left(\frac{\Im\{R_1(1)\}\Re\{R_2(1)\} - \Im\{R_2(1)\}\Re\{R_1(1)\}}{\Re\{R_1(1)\}\Re\{R_2(1)\} + \Im\{R_1(1)\}\Im\{R_2(1)\}}\right), \tag{4.8}$$

where $R_1(1)$ is the complex lag one autocorrelation value for $r_1(i)$ and $R_2(1)$ is the complex lag one autocorrelation value for $r_2(i)$. $\Im$ denotes the imaginary part and $\Re$ the real part.

The approach can, thus, yield the axial and transverse velocity components independently and show the velocity vector. The advantage of the TO method is its fairly low demand on calculations. Both estimators need a modest amount of calculations and the dual or triple beam-former employed by the methods already exists in most high-end scanners of today. Examples from the use of this approach in a commercial scanner can be found in §5.

5. CLINICAL EXAMPLES FOR VECTOR VELOCITY IMAGING

Three examples of typical vector velocity images are shown in figures 7–10. The images were obtained from a Pro Focus 2202 UltraView scanner from BK Medical using a conventional linear array transducer (BK 8670). Around 13–21 frames can be obtained per second in this implementation and unmodified screens shots are shown in the figures.

The first example in figure 7 is from simple unidirectional flow in the jugular vein and the carotid artery. The insonation angle is close to 90° and the vessels are still fully filled with an indication of both direction and magnitude. The colours indicate direction and the length of the arrows indicates velocity magnitude as shown in figure 8.

The second example in figure 9 shows the complex velocity patterns obtained from close to a valve in the femoral vein. The valve closure gives rise to a vortex behind the leaflet, and flow is seen in all directions.

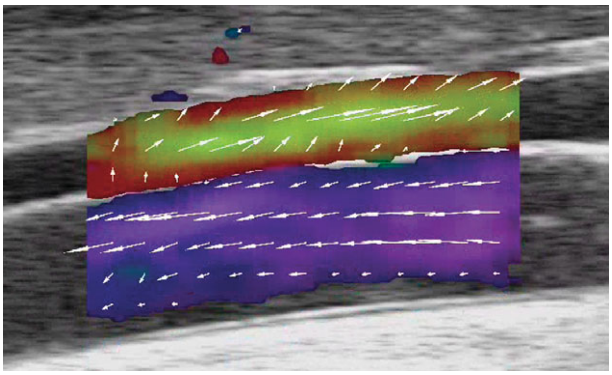

Figure 7. Simple unidirectional flow in the jugular vein (top) and the carotid artery (bottom) (modified figure from Hansen *et al.* [68]).

The final example in figure 10 shows secondary flow in the abdominal aorta. Here, a scan in the transverse plane of the abdominal aorta has been performed and illustrates the rotational motion of the blood in the circumferential direction. This again demonstrates the complexity of the flow that can now be visualized, but also reinforces the point that a full three-dimensional velocity vector estimation is needed for mapping the full picture of the human pulsatile circulation.

A challenge with this type of imaging is the wealth of information presented. Often the flow velocity and direction changes rapidly, which makes it difficult to perceive all details especially around bifurcations and valves where rapid changes are found. For example, the vortex in the carotid bifurcation presented in figure 6 appears after peak systole and disappears within 100–200 ms downstream as the velocity is around 0.4–0.6 m s^{-1}. It is therefore often necessary to inspect slow moving cine-loops or to study still frames as shown in this article to perceive the wealth of information.

6. OTHER EXPERIMENTAL SYSTEMS

Other more advanced vector flow techniques also exist. The synthetic aperture (SA) approach suggested by Nikolov & Jensen [69] is a radical departure from conventional velocity imaging. In conventional CFI systems, data are acquired sequentially one line at a time, and 8–16 emissions have to be performed for each direction, which often lowers the frame rate unacceptably for larger depths. In the SA approach, the image acquisition is continuous using a short sequence of pulse emissions and the whole image is synthesized. The advantage of this method is that data are available from everywhere in the image and that beam formation can be performed in any direction. The continuous imaging makes it possible to average over many emissions to attain standard deviations of around 0.3 per cent [70]. This approach has also been tested clinically and compared with other vector velocity approaches and phased contrast magnetic resonance imaging [71].

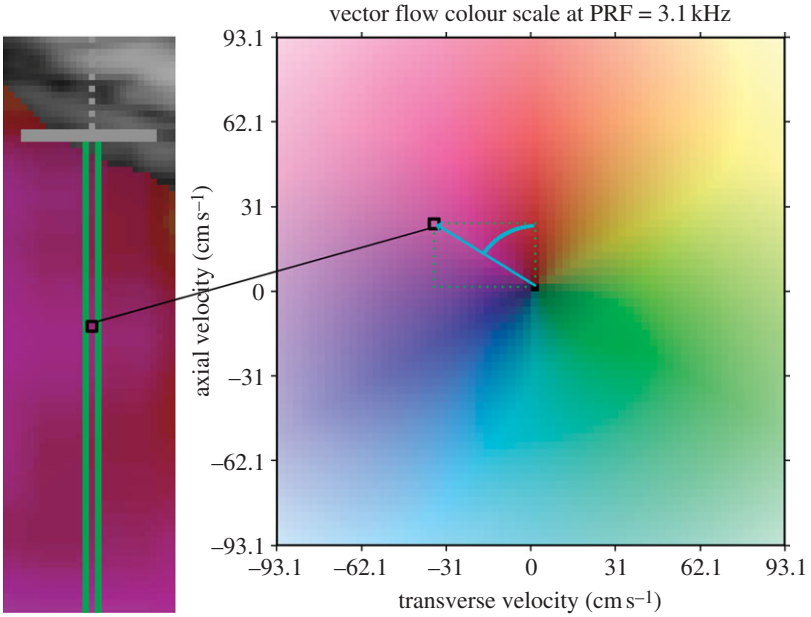

Figure 8. The velocity vector are encoded as both arrows and in a colour scale where the brightness indicates magnitude and the colour direction.

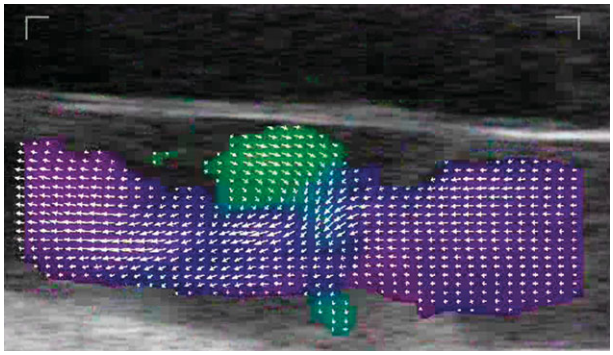

Figure 9. Longitudinal scan of the femoral vein with disturbed flow at the passage of a venous valve. A vortex is formed in the pocket behind the valve (modified figure from Hansen *et al.* [68]).

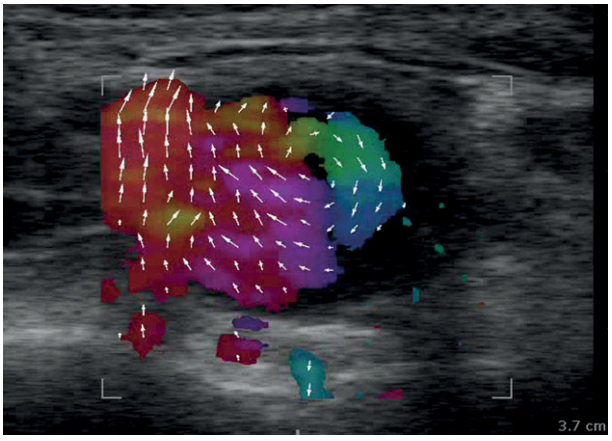

Figure 10. Secondary flow in the abdominal aorta (modified figure from Hansen *et al.* [68]).

Another approach to fast imaging is to employ plane waves, where the images are reconstructed after one or more plane wave emissions. This offers very fast imaging acquisition and can yield frame rates in the kilohertz range. This approach was demonstrated by Udesen *et al.* [72] and several examples of fast imaging using speckle tracking and plane wave emission were shown by Hansen *et al.* [73]. A similar approach using several plane wave emission directions was also demonstrated by Bercoff *et al.* [74]. These approaches demonstrate the fast transitory vortices and other complex flow that can be seen with frame rates of above 100 Hz, which probably also will greatly benefit the studies of cardiac haemodynamics.

7. CONCLUSION

Velocity estimation in medical ultrasound has had a long history since the early work of Satomura [75] on continuous wave Doppler to colour flow mapping introduced by Namekawa *et al.* [31] and Kasai *et al.* [32]. The clinical world has greatly benefited from these safe, fast and interactive systems for studying all parts of the human circulation.

The development of these scanners continues and new methods for vector velocity imaging are on the verge of being introduced. They will add new information to the field allowing the detailed study of complex flow, and they will make the imaging easier as they are angle-independent.

There is no doubt that the development will continue. There is a real need for three-dimensional vector velocity estimation and the frame rate needs to be increased to the 100 Hz range to study complex flow and vortex formation in the heart and other complex anatomical structures.

Tim Hartshorne is thanked for providing the conventional colour flow images, Mads Møller Pedersen and Kristoffer

L. Hansen are thanked for providing the vector velocity images, and BK Medical for providing the ultrasound scanner.

REFERENCES

1 Arning, C., Widder, B., von Reutern, G. M., Stiegler, H. & ôrtler, M. 2010 Revison of DEGUM ultrasound criteria for grading internal carotid artery stenoses and transfer to NASCET measurement. *Ultraschall Med.* **31**, 251–257. (doi:10.1055/s-0029-1245336)

2 Udesen, J., Nielsen, M. B., Nielsen, K. R. & Jensen, J. A. 2007 Examples of *in vivo* blood vector velocity estimation. *Ultrasound Med. Biol.* **33**, 541–548. (doi:10.1016/j.ultrasmedbio.2006.10.014)

3 Thalhammer, C., Aschwanden, M., Mayr, M., Staub, D. & Jaeger, K. A. 2007 Colour-coded duplex sonography after renal transplantation. *Ultraschall Med.* **28**, 6–27. (doi:10.1055/s-2007-962859)

4 Jaeger, K. A. & Uthoff, H. 2010 Is there still a place for renal artery duplex scanning? *Ultraschall Med.* **31**, 339–343. (doi:10.1055/s-0029-1245585)

5 Hamper, U. M., Delong, M. R. & Scoutt, L. M. 2009 Ultrasound evaluation of the lower extremity veins. *Ultrasound Clin.* **4**, 193–216. (doi:10.1016/j.cult.2009.04.003)

6 Parikh, S., Shah, R. & Kapoor, P. 2010 Portal vein thrombosis. *Am. J. Med.* **123**, 111–119. (doi:10.1016/j.amjmed.2009.05.023)

7 Baik, S. K. 2010 Haemodynamic evaluation by doppler ultrasonography in patients with portal hypertension: a review. *Liver Int.* **30**, 1403–1413. (doi:10.1111/j.1478-3231.2010.02326.x)

8 Angelsen, B. A. J., Torp, H., Holm, S., Kristoffersen, K. & Whittingham, T. A. 1995 Which transducer array is best? *Eur. J. Ultrasound* **2**, 151–164. (doi:10.1016/0929-8266(95)00092-5)

9 Thomenius, K. E. 1996 Evolution of ultrasound beamformers. In *Proc. 1996 IEEE Ultrason. Symp., San Antonio, TX, 3–6 November 1996*, pp. 1615–1620. Piscataway, NJ: IEEE.

10 Whittingham, T. A. 2007 Medical diagnostic applications and sources. *Prog. Biophys. Mol. Biol.* **93**, 84–110. (doi:10.1016/j.pbiomolbio.2006.07.004)

11 Jensen, J. A. 1993 Stationary echo canceling in velocity estimation by time-domain cross-correlation. *IEEE Trans. Med. Imag.* **12**, 471–477. (doi:10.1109/42.241874)

12 Brands, P. J., Hoeks, A. P. G., Hofstra, L. & Reneman, R. S. 1995 A noninvasive method to estimate wall shear rate using ultrasound. *Ultrasound Med. Biol.* **21**, 171–185. (doi:10.1016/S0301-5629(94)00111-1)

13 Heimdal, A. & Torp, H. 1997 Ultrasound Doppler measurements of low velocity blood flow: limitations due to clutter signals from vibrating muscles. *IEEE Trans. Ultrason. Ferroelec. Freq. Contr.* **44**, 873–881. (doi:10.1109/58.655202)

14 Fletcher, R. H. & Burlage, D. W. 1972 An initialization technique for improved MTI performance in phased array radars. *IEEE Proc.* **60**, 1551–1552. (doi:10.1109/PROC.1972.8953)

15 Chornoboy, E. S. 1992 Initialization for improved IIR filter performance. *IEEE Trans. Sig. Proc.* **40**, 543–550. (doi:10.1109/78.120797)

16 Peterson, R. B., Atlas, L. E. & Beach, K. W. 1994 A comparison of IIR initialization techniques for improved color doppler wall filter performance. In *Proc. IEEE Ultrason. Symp. Cannes, France, 1–4 November 1994*, pp. 1705–1708. Piscataway, NJ: IEEE.

17 Kadi, A. P. & Loupas, T. 1995 On the performance of regression and step-initialized IIR clutter filters for color Doppler systems in diagnostic medical ultrasound. *IEEE Trans. Ultrason. Ferroelec. Freq. Contr.* **42**, 927–937. (doi:10.1109/58.464825)

18 Tysoe, C. & Evans, D. H. 1995 Bias in mean frequency estimation of Doppler signals due to wall clutter filters. *Ultrasound Med. Biol.* **21**, 671–677. (doi:10.1016/0301-5629(95)00009-G)

19 Hoeks, A. P. G., Hennerici, M. & Reneman, R. S. 1991 Spectral composition of Doppler signals. *Ultrasound Med. Biol.* **17**, 751–760. (doi:10.1016/0301-5629(91)90157-R)

20 Bjærum, S. & Torp, S. 1997 Optimal adaptive clutter filtering in color flow imaging. In *Proc. IEEE Ultrason. Symp., Toronto, Canada, 5–8 October 1997*, pp. 1223–1226. Piscataway, NJ: IEEE.

21 Bjærum, S., Torp, H. & Kristoffersen, H. 2002 Clutter filter design for ultrasound colour flow imaging. *IEEE Trans. Ultrason. Ferroelec. Freq. Contr.* **49**, 204–209. (doi:10.1109/58.985705)

22 Ledoux, L. A. F., Brands, P. J. & Hoeks, A. P. G. 1997 Reduction of the clutter component in Doppler ultrasound signals based on singular value decomposition: a simulation study. *Ultrason. Imag.* **19**, 1–18.

23 Bjærum, S., Torp, H. & Kristoffersen, K. 2002 Clutter filters adapted to tissue motion in ultrasound color flow imaging. *IEEE Trans. Ultrason. Ferroelec. Freq. Contr.* **49**, 693–704. (doi:10.1109/TUFFC.2002.1009328)

24 Kruse, D. E. & Ferrara, K. W. 2002 A new high resolution colour flow system using an eigendecomposition-based adaptive filter for clutter rejection. *IEEE Trans. Ultrason. Ferroelec. Freq. Contr.* **49**, 1739–1754.

25 Løvstakken, L., Bjærum, S., Kristoffersen, K., Haaverstad, R. & Torp, H. 2006 Real-time adaptive clutter rejection filtering in color flow imaging using power method iterations. *IEEE Trans. Ultrason. Ferroelec. Freq. Contr.* **53**, 1597–1608.

26 Yu, A. C. H. & Cobbold, R. S. C. 2008 Single-ensemble-based eigen-processing methods for color flow imaging. Part 1: The Hankel-SVD filter. *IEEE Trans. Ultrason. Ferroelec. Freq. Contr.* **55**, 559–572. (doi:10.1109/TUFFC.2008.682)

27 You, W. & Wang, Y. 2009 Adaptive clutter rejection for ultrasound color flow imaging based on recursive eigendecomposition. *IEEE Trans. Ultrason. Ferroelec. Freq. Contr.* **56**, 2217–2231. (doi:10.1109/TUFFC.2009.1304)

28 Yu, A. & Løvstakken, L. 2010 Eigen-based clutter filter design for ultrasound color flow imaging: a review. *IEEE Trans. Ultrason. Ferroelec. Freq. Contr.* **57**, 1096–1111. (doi:10.1109/TUFFC.2010.1521)

29 Jensen, J. A. 1996 *Estimation of blood velocities using ultrasound: a signal processing approach.* New York, NY: Cambridge University Press.

30 Evans, D. H. & McDicken, W. N. 2000 *Doppler ultrasound, physics, instrumentation, and signal processing.* New York, NY: John Wiley & Sons.

31 Namekawa, K., Kasai, C., Tsukamoto, M. & Koyano, A. 1982 Realtime bloodflow imaging system utilizing autocorrelation techniques. In *Ultrasound '82* (eds R. A. Lerski & P. Morley), pp. 203–208, New York, NY: Pergamon Press.

32 Kasai, C., Namekawa, K., Koyano, A. & Omoto, R. 1985 Real-time two-dimensional blood flow imaging using an autocorrelation technique. *IEEE Trans. Son. Ultrason.* **32**, 458–463.

33 Loupas, T., Powers, J. T. & Gill, R. W. 1995 An axial velocity estimator for ultrasound blood flow imaging, based on a full evaluation of the Doppler equation by means of a two-dimensional autocorrelation approach. *IEEE Trans. Ultrason., Ferroelec., Freq. Contr.* **42**, 672–688.

34 Loupas, T., Peterson, R. B. & Gill, R. W. 1995 Experimental evaluation of velocity and power estimation for blood flow imaging, by means of a two-dimensional autocorrelation approach. *IEEE Trans. Ultrason. Ferroelec. Freq. Contr.* **42**, 689–699. (doi:10.1109/58.393111)

35 Bonnefous, O. 1992 Time domain color flow imaging: methods and benefits compared to Doppler. *Acoust. Imag.* **19**, 301–309.

36 Foster, S. G. 1985 A pulsed ultrasonic flowmeter employing time domain methods. PhD thesis, Department of Electrical Engineering, University of Illinois, Urbana, IL.

37 Embree, P. M. & O'Brien, W. D. 1985 The accurate ultrasonic measurement of volume flow of blood by time-domain correlation. In *Proc. IEEE Ultrason. Symp., San Francisco, CA, 16–18 October, 1985*, pp. 963–966. Piscataway, NJ: IEEE.

38 Bonnefous, O., Pesqué, P. & Bernard, X. 1986 A new velocity estimator for color flow mapping. In *Proc. IEEE Ultrason. Symp.* 855–860. (doi:10.1016/0161-7346(86)90001-5)

39 Bonnefous, O. & Pesqué, P. 1986 Time domain formulation of pulse-Doppler ultrasound and blood velocity estimation by cross correlation. *Ultrason. Imag.* **8**, 73–85. (doi:10.1016/0161-7346(86)90001-5)

40 Dotti, D., Gatti, E., Svelto, V., Uggè, A. & Vidali, P. 1976 Blood flow measurements by ultrasound correlation techniques. *Energia Nucleare* **23**, 571–575.

41 Jensen, J. A. 1993 Implementation of ultrasound time-domain cross-correlation blood velocity estimators. *IEEE Trans. Biomed. Eng.* **40**, 468–474. (doi:10.1109/10.243415)

42 Hein, I. A. & O'Brien, W. D. 1993 Current time-domain methods for assessing tissue motion by analysis from reflected ultrasound echoes: a review. *IEEE Trans. Ultrason. Ferroelec. Freq. Contr.* **40**, 84–102. (doi:10.1109/58.212556)

43 Li, W., van der Steen, A. F. W., Lancée, C. T., Céspedes, I. & Bom, N. 1998 Blood flow imaging and volume flow quantitation with intravascular ultrasound. *Ultrasound Med. Biol.* **24**, 203–214. (doi:10.1016/S0301-5629(97)00275-5)

44 Lipschutz, D. 1998 Combined color flow map and monochrome image. US Patent no. 4761740.

45 Guracar, I. M. 1997 Energy weighted parameter spatial/temporal filter. United States Patent no. 5609155.

46 Pflugrath, L. S. & Souquet, J. 1998 Hand held ultrasonic diagnostic instrument. United States Patent no. 5722412.

47 Wong, K. Y., Banjanin, Z. & Liu, D. C. 1999 Method and system for selectively smoothing color flow images in an ultrasound system. United States Patent no. 5860928.

48 Fox, M. D. 1978 Multiple crossed-beam ultrasound Doppler velocimetry. *IEEE Trans. Son. Ultrason.* **SU-25**, 281–286.

49 Trahey, G. E., Allison, J. W. & von Ramm, O. T. 1987 Angle independent ultrasonic detection of blood flow. *IEEE Trans. Biomed. Eng.* **BME-34**, 965–967. (doi:10.1109/TBME.1987.325938)

50 Kim, H. B., Hertzberg, J. R. & Shandas, R. 2004 Development and validation of echo PIV. *Exp. Fluids* **36**, 455–462. (doi:10.1007/s00348-003-0743-5)

51 Liu, L., Zheng, H., Williams, L., Zhang, F., Wang, R., Hertzberg, J. & Shandas, R. 2008 Development of a custom-designed echo particle image velocimetry system for multi-component hemodynamic measurements: system characterization and initial experimental results. *Phys. Med. Biol.* **53**, 1397–1412. (doi:10.1088/0031-9155/53/5/015)

52 Newhouse, V. L., Censor, D., Vontz, T., Cisneros, J. A. & Goldberg, B. B. 1987 Ultrasound Doppler probing of flows transverse with respect to beam axis. *IEEE Trans. Biomed. Eng.* **BME-34**, 779–788. (doi:10.1109/TBME.1987.325920)

53 Tortoli, P., Guidi, G., Guidi, F. & Atzeni, C. 1994 A review of experimental transverse Doppler studies. *IEEE Trans. Ultrason. Ferroelec. Freq. Contr.* **41**, 84–89. (doi:10.1109/58.265825)

54 Bonnefous, O. 1988 Measurement of the complete (3D) velocity vector of blood flows. In *Proc. IEEE Ultrason. Symp., Chicago, IL, 2–5 October 1988*, pp. 795–799. Piscataway, NJ: IEEE.

55 Jensen, J. A. & Lacasa, I. R. 1999 Estimation of blood velocity vectors using transverse ultrasound beam focusing and cross-correlation. In *Proc. IEEE Ultrason. Symp., Lake Tahoe, NV, 17–20 October 1999*, pp. 1493–1497. Piscataway, NJ: IEEE.

56 Jensen, J. A. 2003 Directional velocity estimation using focusing along the flow direction: I: theory and simulation. *IEEE Trans. Ultrason., Ferroelec., Freq. Contr.* **50**, 857–872.

57 Jensen, J. A. & Bjerngaard, R. 2003 Directional velocity estimation using focusing along the flow direction. II. experimental investigation. *IEEE Trans. Ultrason. Ferroelec. Freq. Contr.* **50** 873–880. (doi:10.1109/TUFFC.2003.1214506)

58 Jensen, J. A. 2004 Velocity vector estimation in synthetic aperture flow and B-mode imaging. *IEEE Int. Symposium on Biomedical Imaging from Nano to Macro, Arlington, VA, 15–18 April 2004*, pp. 32–35. Piscataway, NJ: IEEE.

59 Kortbek, J. & Jensen, J. A. 2006 Estimation of velocity vector angles using the directional cross-correlation method. *IEEE Trans. Ultrason. Ferroelec. Freq. Contr.* **53**, 2036–2049. (doi:10.1109/TUFFC.2006.144)

60 Ohtsuki, S. & Tanaka, M. 2006 The flow velocity distribution from the doppler information on a plane in three-dimensional flow. *J. Visual.* **9**, 69–82. (doi:10.1007/BF03181570)

61 Uejima, T., Koike, A., Sawada, H., Aizaw, T., Ohtsuki, S., Tanaka, M., Furukawa, T. & Fraser, A. G. 2010 A new echocardiographic method for identifying vortex flow in the left ventricle: numerical validation. *Ultrasound Med. Biol.* **36**, 772–788. (doi:10.1016/j.ultrasmedbio.2010.02.017)

62 Tanaka, M., Sakamoto, T., Sugawara, S., Nakajima, H., Kameyama, T., Katahira, Y., Ohtsuki, S. & Kanai, H. 2010 Spiral systolic blood flow in the ascending aorta and aortic arch analyzed by echo-dynamography. *J. Cardiol.* **56**, 97–110. (doi:10.1016/j.jjcc.2010.03.008)

63 Dunmire, B. & Beach, K. W. 2001 A brief history of vector Doppler. In *Proc. SPIE, 4325, Medical Imaging 2001: ultrasonic imaging and signal processing* (eds M. F. Insana & K. K. Shung), pp. 200–214. Bellingham, WA: SPIE.

64 Munk, P. 1996 Estimation of the 2-D flow vector in ultrasonic imaging: a new approach. Master's thesis, Department of Information Technology, Technical University of Denmark.

65 Jensen, J. A. & Munk, P. 1998 A new method for estimation of velocity vectors. *IEEE Trans. Ultrason. Ferroelec. Freq. Contr.* **45**, 837–851. (doi:10.1109/58.677749)

66 Anderson, M. E. 1998 Multi-dimensional velocity estimation with ultrasound using spatial quadrature. *IEEE Trans. Ultrason. Ferroelec. Freq. Contr.* **45**, 852–861. (doi:10.1109/58.677757)

67 Jensen, J. A. 2001 A new estimator for vector velocity estimation. *IEEE Trans. Ultrason. Ferroelec. Freq. Contr.* **48**, 886–894. (doi:10.1109/58.935705)

68 Hansen, P. M., Pedersen, M. M., Hansen, K. L., Nielsen, M. B. & Jensen, J. A. 2011 Examples of vector velocity

imaging. In *Nordic-Baltic Conf. Biomed. Eng. Med. Phys., Aalborg, Denmark, 14–17 June 2011.* IFBME.

69 Nikolov, S. I. & Jensen, J. A. 2003 *In vivo* synthetic aperture flow imaging in medical ultrasound. *IEEE Trans. Ultrason. Ferroelec. Freq. Contr.* **50**, 848–856. (doi:10.1109/TUFFC.2003.1214504)

70 Jensen, J. A. & Nikolov, S. I. 2004 Directional synthetic aperture flow imaging. *IEEE Trans. Ultrason. Ferroelec. Freq. Contr.* **51**, 1107–1118.

71 Hansen, K. L., Udesen, J., Thomsen, C., Jensen, J. A. & Nielsen, M. B. 2009 *In vivo* validation of transverse oscillation vector velocity estimation with MR angiography. *IEEE Trans. Ultrason. Ferroelec. Freq. Contr.* **56**, 91–100. (doi:10.1109/TUFFC.2009.1008)

72 Udesen, J., Gran, F., Hansen, K. L., Jensen, J. A., Thomsen, C. & Nielsen, M. B. 2008 High frame-rate blood vector velocity imaging using plane waves: simulations and preliminary experiments. *IEEE Trans. Ultrason. Ferroelec. Freq. Contr.* **55**, 1729–1743. (doi:10.1109/TUFFC.2008.858)

73 Hansen, K. L., Udesen, J., Oddershede, N., Henze, L., Thomsen, C., Jensen, J. A. & Nielsen, M. B. 2008 *In vivo* evaluation of three ultrasound vector velocity techniques with MR angiography. In *Proc. IEEE Ultrason. Symp., Beijing, China, 2–5 November 2008*, pp. 1060–1063. Piscataway, NJ: IEEE.

74 Bercoff, J., Montaldo, G., Loupas, T., Savery, D., Meziere, F., Fink, M. & Tanter, M. 2011 Ultrafast compound doppler imaging: providing full blood flow characterization. *IEEE Trans. Ultrason. Ferroelec. Freq. Contr.* 134–147.

75 Satomura, S. 1957 Ultrasonic Doppler method for the inspection of cardiac functions. *J. Acoust. Soc. Am.* **29**, 1181–1185. (doi:10.1121/1.1908737)